

# Nanoindentation behavior of nanotwinned Cu: Influence of indenter angle on hardness, strain rate sensitivity and activation volume

In-Chul Choi<sup>a</sup>, Yong-Jae Kim<sup>a</sup>, Y. Morris Wang<sup>b</sup>, Upadrasta Ramamurty<sup>c,d</sup>, Jae-il Jang<sup>a,\*</sup>

<sup>a</sup> Division of Materials Science and Engineering, Hanyang University, Seoul 133-791, Republic of Korea

<sup>b</sup> Physical and Life Sciences Directorate, Lawrence Livermore National Laboratory, Livermore, CA 94550, USA

<sup>c</sup> Department of Materials Engineering, Indian Institute of Science, Bangalore 560012, India

<sup>d</sup> Center of Excellence for Advanced Materials Research, King Abdulaziz University, Jeddah 21589, Saudi Arabia

Received 9 July 2013; received in revised form 14 August 2013; accepted 14 August 2013

Available online 26 September 2013

## Abstract

The influence of strain on the mechanical properties and deformation kinetic parameters of nanotwinned (nt) copper is investigated by a series of nanoindentation experiments, which were performed by employing sharp indenters with five varying centerline-to-face angles ( $\psi$ ). Comparison experiments were also conducted on (110) single crystalline Cu. Experimental results indicate that, unlike coarse-grained materials, nt-Cu is prone to plastic flow softening with large material pile-up around the indentation impression at high levels of strains. Localized detwinning becomes more significant with decreasing  $\psi$ , concomitant with reduced strain-rate sensitivity ( $m$ ) and enhanced activation volume ( $V^*$ ). The  $m$  of nt-Cu is found to depend sensitively on  $\psi$  with a variation of more than a factor of 3, whereas  $V^*$  exhibits a much less sensitive trend. This paper discusses the validation of the experimental techniques and the implications of various deformation kinetic parameters on the underlying deformation mechanisms of nt-Cu.

© 2013 Acta Materialia Inc. Published by Elsevier Ltd. All rights reserved.

**Keywords:** Nanotwinned metals; Nanoindentation; Hardness; Strain-rate sensitivity; Activation volume

## 1. Introduction

Nanocrystalline (nc) metals and alloys (with grain size  $d < 100$  nm) exhibit ultrahigh strength, excellent wear resistance and possibly superplastic formability at low temperatures and/or high strain rates [1]. This far superior mechanical behavior, in comparison with conventional single crystalline (sc) and coarse-grained (cg) metals, is a result of the high concentration of incoherent grain boundaries (GBs) that obstruct dislocation motion. However, the enhanced strength comes at the expense of reduced ductility [2,3]. Compared with ordinary GBs, coherent twin boundaries (TBs) usually exhibit much higher thermal and mechanical stability. Recent studies have shown that the controlled introduction of nanoscale TBs with

spacing  $\lambda < 100$  nm into the microstructure causes significant strengthening (that is quantitatively identical to that from GBs [2]), while preserving acceptable levels of ductility [2,4]. These nanotwinned (nt) metals with nanoscale growth twins also exhibit high thermal stability [5] vis-à-vis incoherent GBs and good electrical conductivity [6].

The strain-rate sensitivity (SRS)  $m$  and the activation volume ( $V^*$ ) are useful quantitative indicators of the predominant mechanism of a stress-assisted, thermally activated plastic deformation process [7–9]. Recent studies have revealed that, similarly to nc metals, nt metals also exhibit an enhanced SRS and reduced  $V^*$  in comparison with their sc and cg counterparts. This elevated SRS may help to delay the necking during tensile deformation and can contribute to ductility. Table 1 provides a summary of the experimental data available in the literature on the  $m$  and  $V^*$  of nt-Cu, a widely examined nt metal, with various  $\lambda$  [1,7,10–12]. Note that the sc and cg-Cu have  $m$

\* Corresponding author.

E-mail address: [jjjang@hanyang.ac.kr](mailto:jjjang@hanyang.ac.kr) (J.-i. Jang).

Table 1  
SRS and activation volume in the literature (T, tension, I, indentation, J, tensile strain rate jump).

$\lambda$ (nm)	$d$ (nm)	Testing method	Strain rate ( $s^{-1}$ )	$m$	$V^*$ ( $b^3$ )	Ref.
~15	~400	T	$\sim 10^{-4}$ – $10^{-1}$	$0.037 \pm 0.014$		[1]
~15	400–500	J	$\sim 10^{-5}$ – $10^{-2}$	0.035–0.046		[10]
~20	~500	I	0.1–100 mN $s^{-1}$	$0.036 \pm 0.009$	~12	[7]
~35	~450	T	$\sim 10^{-4}$ – $10^{-1}$	$0.026 \pm 0.012$		[1]
~40	~3000	I	$\sim 10^{-4}$ – $10^{-2}$	$0.047 \pm 0.003$	$16.1 \pm 2.0$	[11]
40–80	500–600	T	$\sim 10^{-5}$ – $10^{-2}$	0.021		[12]
~90	~500	I	0.1–100 mN $s^{-1}$	$0.025 \pm 0.009$	~22	[7]
~100	400–500	J	$\sim 10^{-5}$ – $10^{-2}$	0.015–0.020		[10]
~100	~425	T	$\sim 10^{-4}$ – $10^{-1}$	$0.012 \pm 0.010$		[1]

values of 0.006 and 0.004–0.007, respectively, and their  $V^*$  is  $\sim 1000b^3$ , where  $b$  is the Burgers vector [13,14]. Table 1 shows that, unless the grain size effect is considered,  $m$  scales inversely with the average  $\lambda$ , which is close to the effects of grain size  $d$  in nc-Cu in previous literature [11,15].

Typically, nanoindentation is employed to evaluate the mechanical properties of nc-/nt-metals [11,16–20]. This is due to the advantages that this technique offers, such as simple procedure and the requirement of only a small volume of material. The latter enables the collection of statistically significant data even on the nc-/nt-metals, whose available sample size is still limited. In particular, nanoindentation is extensively used for examining the SRS behavior of these materials, as indentation strain rates can be varied over four orders of magnitude systematically [17]. Additionally, nanoindentation experiments allow one to explore the deformation behavior of nanostructured materials in a strain range that is well beyond that achievable from tensile tests. These merits made it possible to systematically investigate many factors affecting the SRS of nt metals through nanoindentation experiments. For example, Ye et al. [11] recently analyzed the effects of twin-orientation (to loading direction) and surface polishing on  $m$  of nt-Cu through nanoindentation experiments. It was found that indentation on the plan-view surface (with TBs perpendicular to the loading direction) produces higher  $m$  than that on the cross-sectional surface (with TBs parallel to loading direction) and that the value of  $m$  obtained on the mechanically polished surface (with larger initial dislocation density) is higher than that from the as-deposited surface [11].

Despite the above advantages, however, microstructural instability is often observed during the nanoindentation of nc or nt materials [7,10]. The problem is further compounded by another important but unresolved issue related to  $m$ . It is known that the value of  $m$  in metallic materials depends strongly on the plastic strain level, which could be even more so for nc or nt materials. However, this issue has not yet been examined critically, mainly because of the difficulty in varying strains during nanoindentation tests, wherein a three-sided pyramidal indenter (such as a Berkovich indenter) is routinely employed. Note that the deformation fields underneath a given sharp indenter are affine from the continuum plasticity point of view, because of the geometrical self-similarity of the tip. It is possible to overcome this issue by employing different indenters. The

sharpness of the triangular pyramidal indenter as characterized by its centerline-to-face angle  $\psi$  can be varied. Generally, sharper indenters induce larger strains in the material, owing to the larger volume of material that is displaced [21–24]. Thus, indentations made with different  $\psi$  lead to different levels of strain, allowing a systematic evaluation of the strain effects.

With all the above issues in mind, the present authors explored the influence of the strains on the plastic deformation, SRS and activation volume of nt-Cu through a series of nanoindentation experiments using five different indenters with various  $\psi$ . In addition, the tests under the identical condition were carried out on (110) sc-Cu for comparison purposes. The results reveal that the nature of plastic flow in nt-Cu is significantly affected by the level of applied strain, which is discussed in terms of changes in rate-sensitive deformation mechanism and microstructures underneath the indenter.

## 2. Experimental

A  $\sim 170 \mu\text{m}$  thick nt-Cu foil was prepared by layer-by-layer deposition of high-purity ( $>99.99\%$ ) Cu onto a (100) silicon wafer through DC magnetron sputtering. Details of this procedure are similar to those described in Ref. [12]. The grains are columnar in nature, and their diameter is of the order of 0.5–3.0  $\mu\text{m}$  with a twin lamella spacing ranging between 40 and 80 nm. For comparison purposes, the (110) facet of sc-Cu was also examined. The sample surfaces were initially ground with fine SiC papers and gently polished with a microcloth, using 0.3  $\mu\text{m}$  alumina. The sample was given a final electrolytic polishing to remove any possible surface damage induced during prior mechanical polishing.

Nanoindentation experiments were performed at room temperature using a Nanoindenter-XP (formerly MTS; now Agilent, Oak Ridge, TN). Five different three-sided pyramidal indenters with centerline-to-face angles  $\psi$  of  $35.3^\circ$  (cube-corner),  $50^\circ$ ,  $65.3^\circ$  (Berkovich),  $75^\circ$  and  $85^\circ$  were employed. During the tests, the specimen was loaded to a fixed peak load,  $P_{\text{max}} = 100 \text{ mN}$ , with indentation strain rates  $\dot{\epsilon}_i (=h^{-1}(dh/dt))$  and is equal to half the loading rate  $P^{-1}(dP/dt)$  [25]) of 0.01, 0.025, 0.05 and  $0.125 \text{ s}^{-1}$ . For each combination, more than 30 tests were conducted, so as to obtain statistically significant hardness values.

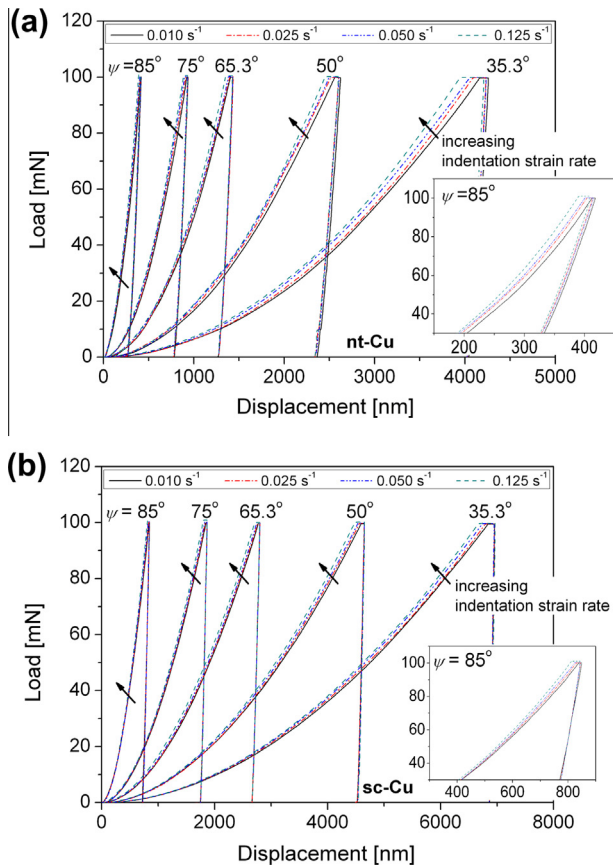


Fig. 1. Variations in load–displacement curves obtained at different indentation rates with various indenters: (a) nt-Cu; (b) sc-Cu.

Thermal drift was maintained  $<0.1 \text{ nm s}^{-1}$  in all experiments. The hardness impressions were imaged using a field-emission scanning electron microscopy (FE-SEM), JSM-6330F (JEOL Ltd., Tokyo, Japan). The topological graph of the indented surface was measured by an atomic force microscopy (AFM), XE-100 (Park Systems, Suwon, Korea). The indentation direction for nt-Cu was vertical to the growth plane.

In order to observe microstructural changes, if any, that occur as a result of the deformation right underneath the indenter, specimens for transmission electron microscopy (TEM) were prepared by focused ion beam milling with Nova 200 NanoLab (FEI Co, Hillsboro, OR). At around the vertex of the indented impression, a thin slice was milled and lifted. To minimize the possibility of beam-induced heating, the Ga ion beam intensity and acceleration voltage were kept as low as 10 pA and 30 kV, respectively. TEM was performed in the scanning mode as well as the high-resolution mode, with the aid of a Tecnai F20 instrument (FEI Co., Hillsboro, OR).

### 3. Results

#### 3.1. Load–displacement curves and plasticity

Fig. 1a shows the representative load–displacement ( $P$ – $h$ ) plots obtained on nt-Cu with different indenters and at

different  $\dot{\epsilon}_i$  with  $P_{\max} = 100 \text{ mN}$ . Corresponding plots obtained on sc-Cu are displayed in Fig. 1b. For clarity, the top segments of the curves for  $\psi = 85^\circ$  are magnified in the inset. For both nt-Cu and sc-Cu, the displacement at the peak load  $h_{\max}$  increases with decreasing  $\psi$ . Importantly, significant rate dependence was observed in nt-Cu, with  $h_{\max}$  decreasing as  $\dot{\epsilon}_i$  increased for any given value of  $\psi$ . However, such rate dependence is clearly less pronounced for sc-Cu.

The ratio of the residual displacement after complete unloading  $h_f$  to  $h_{\max}$  is an indicator of the relative portion of the plastic deformation in the total elasto-plastic deformation that occurs during indentation. The variations in  $h_f/h_{\max}$  with  $\dot{\epsilon}_i$  are summarized in Fig. 2, which indicate the following. For a given  $\dot{\epsilon}_i$ – $\psi$  combination, the  $h_f/h_{\max}$  value obtained on nt-Cu is much lower than that measured on sc-Cu, which implies that plasticity in the former is less pronounced than in the latter. In both the cases, a higher  $h_f/h_{\max}$  is obtained with a sharper indenter and for faster indentation.

#### 3.2. Hardness variation

From the  $P$ – $h$  curves, values of nanoindentation hardness  $H_{O-P}$  were estimated according to the Oliver–Pharr (O–P) method [26]. The area function for each indenter (which is essential to calculate the hardness) was

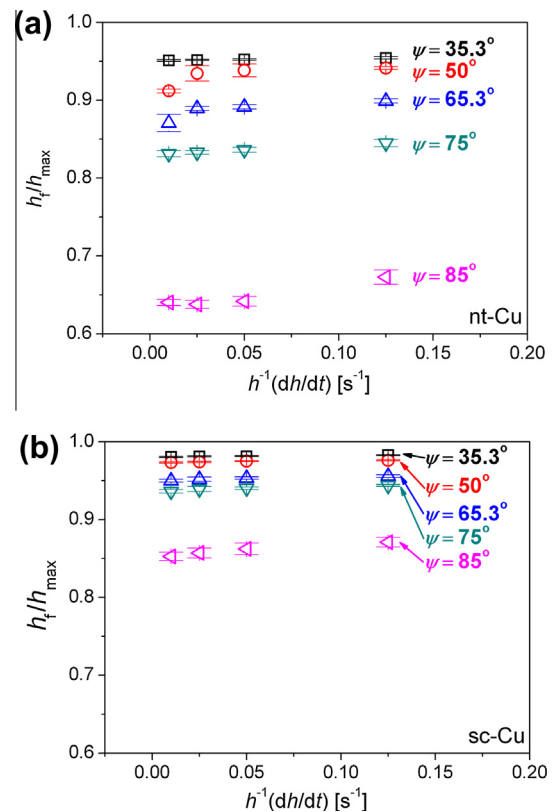


Fig. 2. Changes in the ratio of the final depth to the maximum displacement as a function of indentation rate: (a) nt-Cu; (b) sc-Cu.

determined through preliminary indentation tests made on fused quartz. Variations in  $H_{O-P}$  with  $\psi$  for both nt- and sc-Cu are displayed in Fig. 3. The hardness of nt-Cu obtained with the Berkovich indenter ( $\psi = 65.3^\circ$ ),  $2.44 \pm 0.038$  GPa, is in a good agreement with the literature data [5,7,11,27,28], while no comparable data for other indenter angles are currently available in the literature. The hardness of sc-Cu obtained from Berkovich indentations,  $0.541 \pm 0.004$  GPa, is slightly lower than that reported by Vlassak and Nix [29], which may be due to either indentation size effect ( $h_{max}$  is  $\sim 1000$  nm in Ref. [29], whereas it is  $\sim 2000$  nm in the present study) or different surface preparation methods (mechanical polishing in Ref. [29] and electrolytic polishing in the present study).

In Fig. 3, two trends are obvious from the results on nt-Cu. First, as expected from the  $P-h$  curves in Fig. 1a, the  $H_{O-P}$  for each indenter is unambiguously rate sensitive and increases with increasing  $\dot{\epsilon}_i$ . In contrast,  $H_{O-P}$  is insensitive to  $\dot{\epsilon}_i$  in the case of sc-Cu. Second, the  $H_{O-P}$  increases with decreasing  $\psi$ , except for  $\psi = 35.3^\circ$  whose  $H_{O-P}$  value is lower than that for  $\psi = 50^\circ$ . For sc-Cu,  $H_{O-P}$  decreases linearly with  $\dot{\epsilon}_i$  throughout the entire range of  $\psi$  investigated. This is the expected trend in metals and alloys that exhibit strain hardening.

It is possible that the trends for nt-Cu are conceivably an artifact arising from the uncertainty about the applicability of the O-P method [26] to various indenter angles. For example, the correlation constant  $\beta$  (which relates stiffness  $S$  to area  $A$  and is therefore important for determining the area function and thus the  $H_{O-P}$ ) is known only for the commonly used Berkovich indenter (as a constant of 1.034 [30]), and the dependence of the  $\beta$  value on the indenter angle is still unclear, although some work on this has been done [31]. This may result in miscalculations of the hardness data for other indenters adopted in this study. To examine this critically, the Mayer's hardness  $H_M$  was estimated by measuring the impression size (or contact area)  $A$  directly from a large number of SEM images for  $\psi = 35.3, 50, 65.3$  and  $75^\circ$  (see Fig. 4). Note that the con-

tact area for  $\psi = 85^\circ$  could not be measured because of the difficulty in identifying the true edge of the impression, which is a result of the relatively shallow indentation depth in this case. Values of  $A$  are listed in Table 2.  $H_M$  is then estimated using the following relation:

$$H_M = h_{max}/A = 4h_{max}/(3\sqrt{3}a^2) \quad (1)$$

where  $a$  is the average length measured from the center of the triangular impression to the corner.  $H_M$  and  $H_{O-P}$  are compared in Fig. 5 for both nt-Cu and sc-Cu. As expected,  $H_M$  and  $H_{O-P}$  of sc-Cu are identical. In contrast,  $H_M$  is lower than  $H_{O-P}$  in the case of nt-Cu. The trends in  $H_M$  and  $H_{O-P}$  with  $\psi$  are somewhat similar; in particular,  $H_M$  of nt-Cu for  $\psi = 35.3^\circ$  is indeed lower than that for  $\psi = 50^\circ$  (like  $H_{O-P}$ ), supporting the view that the trend of nt-Cu seen in Fig. 3 is not an artifact. While  $H_M$  and  $H_{O-P}$  are almost identical for sc-Cu,  $H_M$  of nt-Cu is slightly lower than its  $H_{O-P}$ . This may be because of the material pile-up around the indentation (which is pronounced only in nt-Cu, as discussed below), which is not taken into consideration in the O-P method and thus can induce an over-estimated  $H_{O-P}$  [32,33].

### 3.3. Indentation morphology

Representative SEM micrographs of the indents displayed in Fig. 4 show no cracking in any of the indentations, suggesting fully plastic flow in nt- and sc-Cu. In the latter case, no pile-up could be seen. In contrast, the pile-up behavior in nt-Cu was found to be sensitive to  $\psi$ . For  $\psi \geq 65.3^\circ$ , there was little pile-up. In contrast, significant pile-up is seen for  $\psi \leq 50^\circ$ , and the pile-up becomes pronounced with decreasing  $\psi$ . For sharper indenters (especially,  $\psi = 35.3^\circ$ ), the morphology of the pile-up is that of shear-off steps, indicating inhomogeneous or localized plastic flow. These features are similar to those reported in nc alloys as well as metallic glasses [34]. Trelawicz and Schuh [17], who investigated Ni-W alloy as a function of the grain size  $d$ , observed that, in nc-metals with very small  $d$  ( $< \sim 10$  nm), the pile-up becomes inhomogeneous (i.e., plastic flow is shear band mediated, just as in metallic glasses), activation volume increases and SRS decreases, which is similar to what was observed here for small  $\psi$ .

Fig. 6 shows the representative AFM images of selected indents and line scans across them in nc- and sc-Cu samples. The inhomogeneous nature of the pile-up in nt-Cu is evident with steps on the line scan of nt-Cu (Fig. 6a). Even from the same cube-corner indenter, the pile-up behavior is almost negligible for sc-Cu (Fig. 6b). From the AFM surface profile data, the ratio of pile-up height  $h_{pile-up}$  to  $h_{max}$  for each indenter was measured, and the results are summarized in Fig. 7. This ratio is negligible for sc-Cu and is almost  $\psi$ -independent. In contrast, the  $h_{pile-up}/h_{max}$  ratio is significant in the case of nt-Cu.

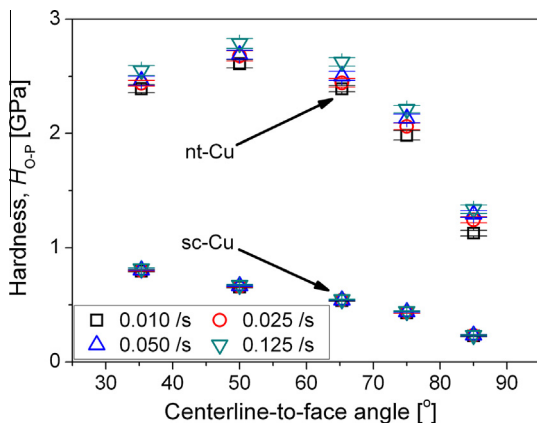


Fig. 3. Nanoindentation hardness (estimated according to the O-P method) for different indenter angles.

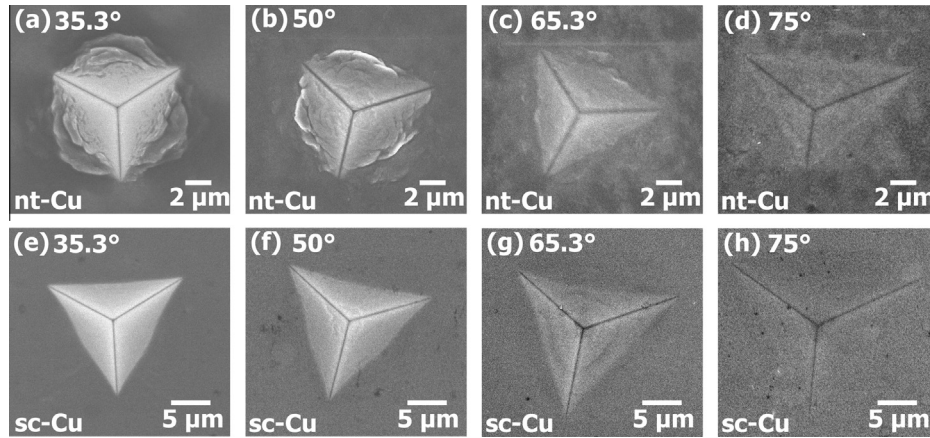


Fig. 4. Representative SEM micrographs of hardness impressions produced with different indenters (at a peak load of 100 mN and indentation strain rate of  $0.025 \text{ s}^{-1}$ ): (a–d) for nt-Cu; (e–h) for sc-Cu.

Table 2

Contact area  $A$  measured using SEM micrographs (for the peak load of 100 mN and indentation strain rate of  $0.025 \text{ s}^{-1}$ ).

		35.3°	50°	65.3°	75°
nt-Cu	$A$ ( $\mu\text{m}^2$ )	$42.81 \pm 0.54$	$41.13 \pm 0.84$	$48.54 \pm 1.72$	$55.70 \pm 2.50$
sc-Cu	$A$ ( $\mu\text{m}^2$ )	$124.7 \pm 1.17$	$149.39 \pm 2.15$	$179.37 \pm 3.19$	$225.53 \pm 7.75$

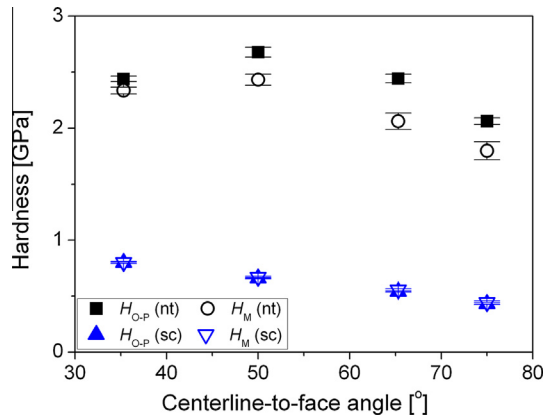


Fig. 5. Comparison of  $H_M$  and  $H_{O-P}$  (obtained at a peak load of 100 mN and an indentation strain rate of  $0.025 \text{ s}^{-1}$ ).

## 4. Discussion

### 4.1. Stress–strain responses

The  $H$  vs.  $\psi$  data are converted into stress vs. strain, which gives insights into the plastic flow behavior of nt-Cu as follows. To convert  $H$  into flow stress  $\sigma_{f,i}$ , the well-known empirical relationship originally suggested by Tabor [35] is employed:

$$H = C_\theta \cdot \sigma_{f,i} \quad (2)$$

where  $C_\theta$  is the constraint factor, which is typically in the range of 2.6–3.0 [35,36] for metallic materials in the fully plastic regime of indentation. However, the validation of the constraint factor to nc or nt material has recently become questionable, owing to the significantly different

strain hardening behavior of these materials and uncertainties arising from tensile results [37]. It is thus important to address this issue for the nt-Cu tested here. Furthermore,  $C_\theta$  would be a strong function of  $\psi$  in the elasto-plastic regime [38]. In this regime, Johnson [38] estimated  $C_\theta$  as

$$C_\theta = \frac{2}{3} \left[ 1 + \ln \left( \frac{E}{\sigma_y} \cdot \cot \theta \right) \right] \quad (3)$$

where  $E$  is the elastic modulus,  $\sigma_y$  is the yield strength, and  $\theta$  is the half-angle of a conical indenter. It is possible to relate the conical indentation used in Eq. (3) to the triangular pyramidal indentation used in the current work by assuming that identical indentation responses are obtained when  $\theta$  gives the same area-to-depth ratio as the pyramid, which gives the relation between  $\psi$  and  $\theta$  as

$$\theta = \tan^{-1} \left( \sqrt{\frac{3\sqrt{3}}{\pi}} \cdot \tan \psi \right) \quad (4)$$

Thus,  $\psi = 35.3, 50, 65.3, 70$  and  $85^\circ$  would correspond to  $\theta = 42.3, 56.9, 70.3, 74.2$  and  $86.1^\circ$ , respectively. With these  $\theta$  values and  $E$  ( $\sim 110$  GPa for nt-Cu [1];  $\sim 130$  GPa for sc-Cu [29]) and  $\sigma_y$  ( $\sim 0.6$  GPa for nt-Cu [12];  $\sim 0.068$  GPa for sc-Cu [39]) obtained from the literature,  $C_\theta$  is estimated using Eq. (3). Only the case of  $\psi = 85^\circ$  for nt-Cu exhibits a low value of  $C_\theta$  ( $\sim 2.4$ ), and all other cases show  $C_\theta > 3$ . Thus, it is considered that  $C_\theta = 3$  (following Johnson [38]) except for the case of  $\psi = 85^\circ$  for nt-Cu. With these  $C_\theta$ ,  $H_{O-P}$  is converted into  $\sigma_{f,i}$ . Note that  $H_{O-P}$  is used instead of  $H_M$  simply because proper SEM images could not be obtained for  $\psi = 85^\circ$ .

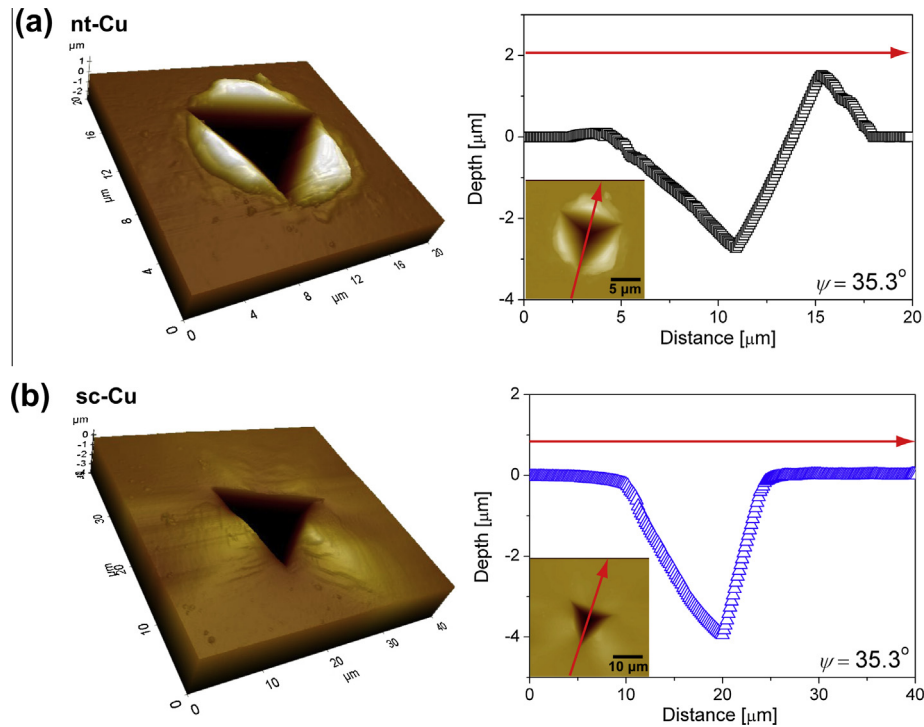


Fig. 6. Representative examples of AFM images and surface profile data from cube-corner indentation of (a) nt-Cu and (b) sc-Cu.

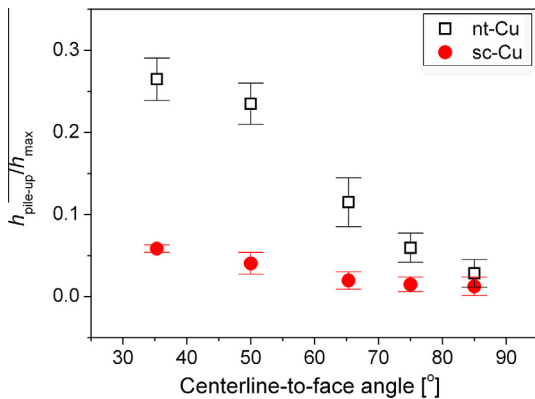


Fig. 7. Change in the ratio of the pile-up height to the maximum displacement.

For the indentation or characteristic strain ( $\varepsilon_{\text{char}}$ ) associated with each sharp indenter geometry, Johnson's [38] often-used relationship is employed:

$$\varepsilon_{\text{char}} = 0.2 \cdot \cot \theta \quad (5)$$

which is derived on the basis of an expanding cavity analogy. Note that a similar equation (with 0.22 as a multiplier instead of 0.2 in Eq. (5)) was also suggested by Sakai et al. [40], who conducted finite-element analyses for elastic–perfectly plastic and elastic–linear strain hardening conical indentations. Eq. (5) leads to  $\varepsilon_{\text{char}}$  value for  $\psi = 85, 75, 65.3$  (Berkovich), 50 and  $35.3^\circ$  (cube-corner) as 0.014, 0.042, 0.072, 0.13 and 0.22, respectively. These strain values suggest that the present nanoindentation experiments explore a wide range of strain behavior in nt-Cu. Variation

of flow stress with characteristic strain for both nt- and sc-Cu is plotted in Fig. 8. It is noted that there is a large increase in  $\sigma_{f,i}$  of nt-Cu, from  $\sim 0.5$  GPa at  $\varepsilon_{\text{char}} = 0.014$  to  $\sim 0.9$  GPa at  $\varepsilon_{\text{char}} = 0.13$ , indicating that nt-Cu can strain harden in a substantial manner. Power-law fitting of the data in the  $\varepsilon_{\text{char}}$  range 0.014–0.13 (i.e.,  $\psi$  of  $85$ – $50^\circ$ ) yields the strain hardening exponent  $n$  (of  $\sigma \propto \varepsilon^n$ ) of 0.23–0.27 (depending on the indentation strain rate). These  $n$  values are remarkably close to  $\sim 0.28$  from the tensile test in Fig. 1 of Ref. [1], implying that the estimated stress–strain behavior by the method described here is meaningful.

As mentioned earlier, when the characteristic strains are increased further to 0.22 (i.e.,  $\psi$  of  $35.3^\circ$ ), flow softening is seen. Mirshams and Pothapragada [41], who performed

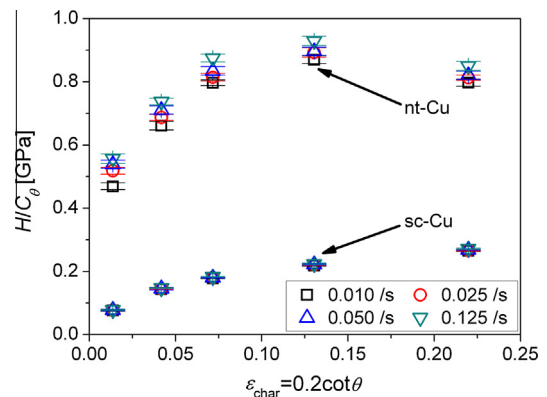


Fig. 8. Stress–strain relation estimated from nanoindentation experiments.

nanindentation tests on nc-Ni with Berkovich and cube-corner indenters, reported that  $H_{O-P}$  obtained with the cube-corner indenter was much lower than that obtained with the Berkovich indenter. They speculated that this softening behavior for  $\psi = 35.3^\circ$  might be related to some role of GBs, but no detailed mechanisms were given. For nt-Cu, earlier nanindentation experiments using the Berkovich tip [27] suggested that TBs are much more stable than nc grains, which can grow under nanindentation, leading to strong softening [42]. Although tensile tests of similar nt-Cu (Fig. 2 in Ref. [12]) also revealed a softening behavior after yielding, the softening observed at high strains in the present work nonetheless remains intriguing as the nanindentation direction is vertical to the TBs (i.e., hard deformation mode), in which case strong strain hardening is expected [11,43] (which is consistent with the  $n$  values calculated above). To explore the possible mechanisms of this softening behavior, the present authors investigated the potential microstructure change underneath the indenter for Berkovich ( $\psi = 65.3^\circ$ ) and cube-corner tips ( $\psi = 35.3^\circ$ ), as shown in the cross-sectional TEM images in Fig. 9. Observation of the deformation underneath the indenter is important, since the deformation mechanism near the unconstrained surface plays a less important role during nanindentation of nc materials than that underneath the indenter [44]. Note that the subsurface region underneath the hardness impression (Fig. 9a and b) exhibits quite different microstructures from that of undeformed region shown in Fig. 9c. Two features stand out in the figure. First, the collapse of the twin structure occurred during indentation (i.e., detwinning) in both indenters. Second, the collapsed region (i.e., detwinning area) for cube-corner indentation is much larger than that for Berkovich indentation, which may be due to the higher strains underneath sharper indenter. These results demonstrate that detwinning does occur underneath the indenter, probably caused by the intrinsically defective structures of TBs, as suggested by recent TEM and in situ synchrotron diffraction studies [45]. The present authors hypothesize that the softening behavior for the cube-corner indentation is associated with this large amount of detwinning structures. In cube-corner indentation, large plastic strain produced underneath the indenter cannot be fully accommodated by surrounding nanotwin structures. As such, the material pile-up around hardness impression can be more pronounced. The TEM image shown in Fig. 9d further indicates that no twin structure is observable in the pile-up region from the cube-corner indentation. These experimental results, although in contrast to some earlier reports [27], confirm that the detwinning process can occur during nanindentation, which seems to become more severe at larger strains (i.e., using the cube-corner indenter whose  $\varepsilon_{\text{char}}$  is 0.22). The localized detwinning processes observed here are, nonetheless, consistent with some other observations in the literature [46–48]. Note that the strain levels involved in the nanindentation experiments and the grain boundary structure of the present materials (which is considered

critically relevant to the detwinning process [45]) are substantially different from those reported in Ref. [27]. The nanindentation-induced change in microstructure suggests that caution is needed when one interprets the quantitative data acquired by different indenters (to be discussed in the next section).

Another possibility can be found in the previous MD simulation study of Shabib and Miller [49], who showed that, after the strengthening effect reaches a maximum, large numbers of dislocations begin to cross the TBs, and thus the stress starts to decrease. However, in the present study, the authors could not find any experimental evidence for this scenario of dislocation transfer through TBs.

#### 4.2. SRS, activation volume and deformation mechanism

As mentioned earlier,  $m$  is an important material property, which enables an understanding of thermally activated plastic deformation mechanisms, and is often determined at a given strain  $\varepsilon$  and temperature  $T$  by relating uniaxial flow stress  $\sigma_f$  and strain rate  $\dot{\varepsilon}$  [50]:

$$m = \left( \frac{\partial \ln \sigma_f}{\partial \ln \dot{\varepsilon}} \right)_{\varepsilon, T} \quad (6)$$

For indentation,  $\sigma_f$  can be set as  $\sigma_{f,i}$ , whereas  $\dot{\varepsilon}$  and the indentation strain rate  $\dot{\varepsilon}_i$  are related through the empirical relation  $\dot{\varepsilon} \sim 0.01 \dot{\varepsilon}_i$  [51]. Thus,  $m$  values at various  $\varepsilon_{\text{char}}$  have been estimated from the slopes of the double logarithmic plots of  $H/C_\theta$  vs.  $\dot{\varepsilon}_i$  displayed in Fig. 10a and b (for nt-Cu and sc-Cu, respectively). It is important to note that the  $m$  measured from nanindentations at different  $\dot{\varepsilon}_i$  (as in this study) are often much smaller than those estimated from the nanindentation creep data by simple conversion,  $m = 1/n$ , where  $n$  is the creep stress exponent of  $\dot{\varepsilon} = K(\sigma)^n$ . However, the inverse relation between  $n$  and  $m$  may not be valid, because stress states used for determining  $n$  and  $m$  are substantially different from each other [52–54].

The variation in  $m$  with  $\varepsilon_{\text{char}}$  is displayed in Fig. 10c, where the Berkovich indentation data (for sc-, cg- and nc-Cu) obtained by Chen et al. [16] are also shown for comparison purposes. It is seen that the value of  $m$  estimated in the present work ( $\sim 0.036$ ) for nt-Cu and sc-Cu (0.006) are within the range reported in the literature (see Table 1 [1,7,10–12]). In Fig. 10c, the  $m$  values in Ref. [16] for nc-Cu (with  $d$  of  $\sim 40$  nm), cg-Cu ( $d > 100$   $\mu\text{m}$ ) and (123) sc-Cu are in a good agreement with the present results; i.e.,  $m$  for sc-Cu is similar to that found in the present study, and  $m$  for cg-Cu is slightly higher than that for sc-Cu. It is noteworthy that nt-Cu with a twin spacing  $\lambda$  of 40 nm in the present study has higher  $m$  than nc-Cu with similar  $d$  [16].

It is also evident in Fig. 10c that the  $m$  is sensitive to  $\varepsilon_{\text{char}}$ , with  $m$  reducing markedly from 0.07 to 0.025 as  $\varepsilon_{\text{char}}$  increases from 0.014 to 0.13. In the flow softening regime, i.e.,  $\varepsilon_{\text{char}} \geq 0.13$ ,  $m$  remains invariant at  $\sim 0.025$ . In contrast, for sc-Cu,  $m$  essentially remains invariant, and mostly

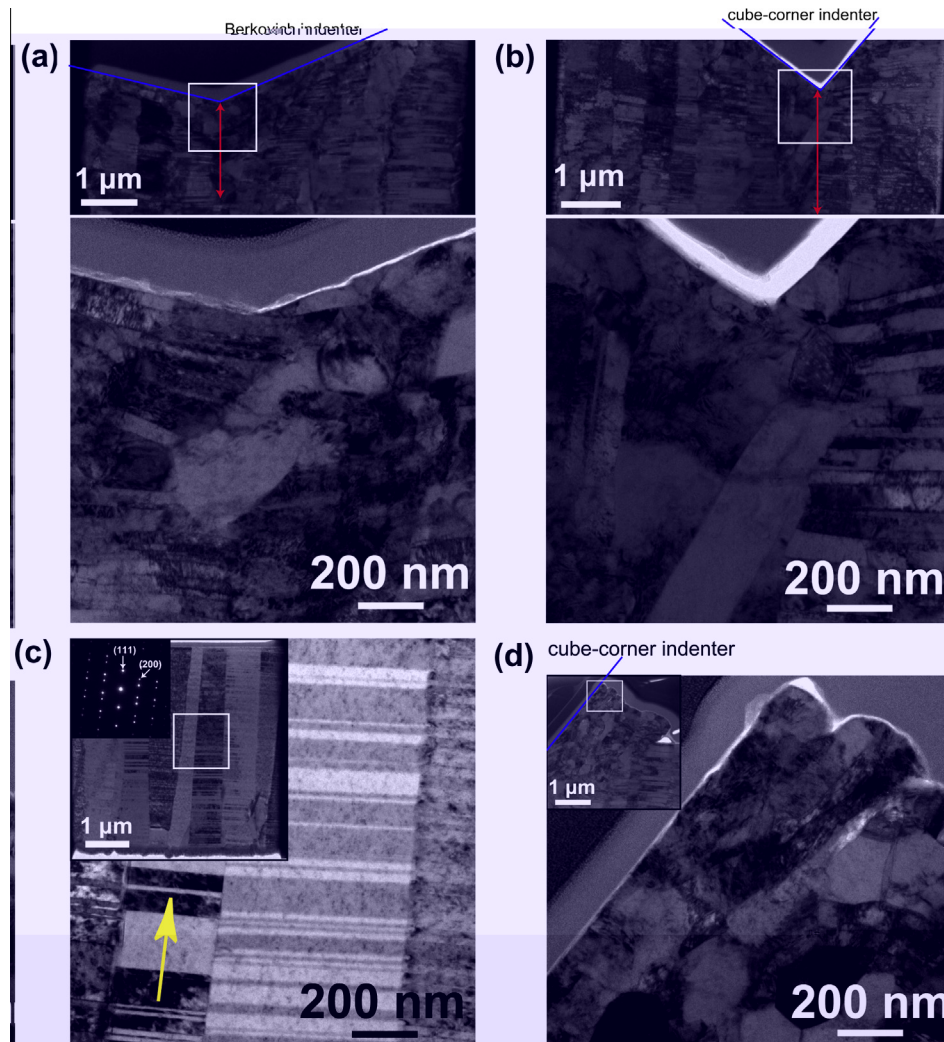


Fig. 9. Cross-sectional TEM micrographs for the subsurface region underneath the impression of nt-Cu for (a) the Berkovich indenter and (b) the cube-corner indenter; (c) undeformed nt-Cu examined from (110) zone axis (in which inserted arrow shows growth direction) with inset of selected area diffraction pattern; (d) the pile-up region for the cube-corner indentation.

very low ( $< \sim 0.01$ ), throughout the range of  $\varepsilon_{\text{char}}$  examined in the present work. The dependence of  $m$  on  $\varepsilon_{\text{char}}$  in nt-Cu is expected, as SRS is known to be a function of deformation strains in face-centered cubic (fcc) nanostructured metals [55]. However, the magnitude of variation (a factor of more than 3) obtained by various indenters here is surprising, suggesting the critical importance of selecting proper indenters and indentation conditions when reporting  $m$  for various nanostructured materials. In a relevant study, the strain dependence of  $m$  in a nt-Cu sample (with average twin lamellar spacing of  $15 \pm 7$  nm) was reported by Shen et al. [10], who evaluated the change in  $m$  with strain rate and plastic strain through tensile strain rate jump tests. It was found that  $m$  decreases slightly with strain from  $\sim 0.046 \pm 0.006$  at  $\varepsilon \approx 0.012$  to  $\sim 0.034 \pm 0.006$  at  $\varepsilon \approx 0.03$  [10]. While the strain range examined in Ref. [10] is limited (0.01–0.03), the strain dependence of  $m$  is in reasonable agreement with the present data for  $\varepsilon_{\text{char}}$  ranging from 0.014 to 0.072. Shen et al. [10] attribute this behavior to the increase in deforma-

tion-induced twin spacing. In a separate study using nano-indentation, Ye et al. [11] discovered increased  $m$  in a polished nt-Cu sample ( $\gamma \approx 40$  nm) containing higher dislocation density, suggesting that  $m$  is generally enhanced with strain if twin spacing is unmodified. The results in Fig. 10 suggest decreasing  $m$  with increasing strains. However, as discussed above, detwinning occurs in the samples when small  $\psi$  indenters are used ( $< 65.3^\circ$ ), i.e., the measured  $m$  values under small  $\psi$  may not be representative of the initial microstructure.

With  $m$ , the activation volume  $V^*$ , which is defined as

$$V^* = \sqrt{3}kT \left( \frac{\partial \ln \dot{\varepsilon}}{\partial \sigma_f} \right) = C_\theta \sqrt{3}kT \left( \frac{\partial \ln \dot{\varepsilon}}{\partial H} \right) \quad (7)$$

where  $k$  is the Boltzmann constant, and  $T$  is the absolute temperature, also provides a useful clue for the plastic deformation mechanism of metals, since it can vary by orders of magnitude for different rate-limiting processes [56]. The typical magnitude of  $V^*$  for the forest dislocations cutting mechanism in sc or cg metals (especially with fcc struc-

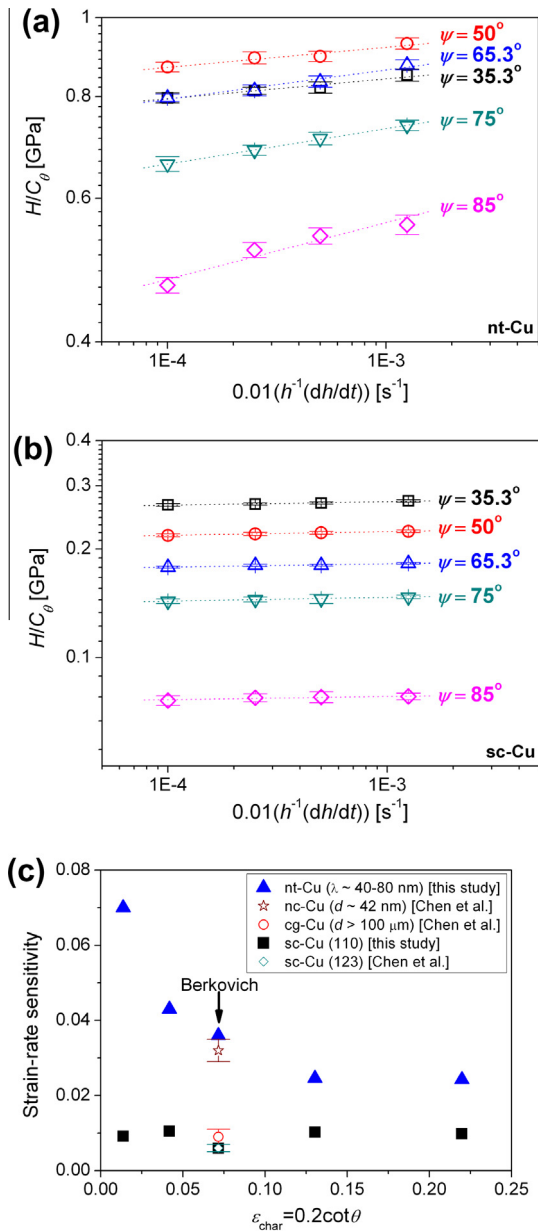


Fig. 10. Estimation of SRS: Stress vs. strain rate for (a) nt-Cu and (b) sc-Cu; (c) summary of estimated SRS. Literature data from Ref. [16] are included for comparison purposes.

ture) is of the order of several hundred to a couple of thousand time  $b^3$  [57]. In nc metals, the  $V^*$  for dislocation-mediated flow is known to be reduced to the order of several tenths  $b^3$ , since dislocation nucleation sources are changing from a typical Frank–Read source to GBs [8,58]. In this case, the plastic flow is accommodated by the interaction of dislocations with various boundaries, such as GBs. In nt metals, slip behavior are mediated by TBs, and thus reduced  $V^*$  is observed, according to small average  $\lambda$  [56]. According to Eq. (7), the  $V^*$  values of nt-Cu could be estimated from the slope of the linear fit of logarithmic strain rate vs. linear flow stress in Fig. 11a. The results are summarized in Fig. 11b where, with increasing indenter angle, the  $V^*$  of the nt-Cu increases mildly with reducing  $\psi$  (from

$\sim 12b^3$  for  $\psi = 85^\circ$  to  $\sim 20b^3$  for  $\psi = 35.3^\circ$ ). The  $V^*$  for the sc-Cu (not shown here) is in the range  $\sim 200\text{--}500b^3$  (which is in agreement with the literature data [16]) and does not exhibit meaningful change with  $\psi$  as one might expect from the angle-independent  $m$  values. The estimated  $V^*$  values clearly show a smaller variation trend than  $m$ , and may suggest that the main deformation mechanism for different indenters remains in the regime of TB-mediated dislocation flow. This qualitative picture, however, cannot accurately describe the relatively complex microstructure evolutions observed in the present TEM experiments, suggesting that  $V^*$  alone is insufficient to infer the complete deformation mechanisms. The slightly larger  $V^*$  under smaller  $\psi$  is not surprising, considering the far more coarsened post-indentation microstructure (i.e., detwinning) for smaller  $\psi$ .

Values of equivalent strain,  $m$  and  $V^*$  are summarized in Table 3, which indicates a relatively high  $m$  ( $=0.07$ ) at small strains (e.g., 0.014) compared with much smaller  $m$  ( $=0.025$ ) at high strains (e.g., 0.22). However, the variation  $V^*$  is observed to be modest. This behavior could be qualitatively related to several different deformation mechanisms in nt-Cu that have been proposed in the literature; namely, the dislocation emission/nucleation from stress concentrators of GBs or TBs [9], channeling of dislocations within twin lamella [11] and slip-transfer of dislocation through TBs [56]. Owing to the complex and inhomogeneous stress/strain states that prevail underneath a sharp

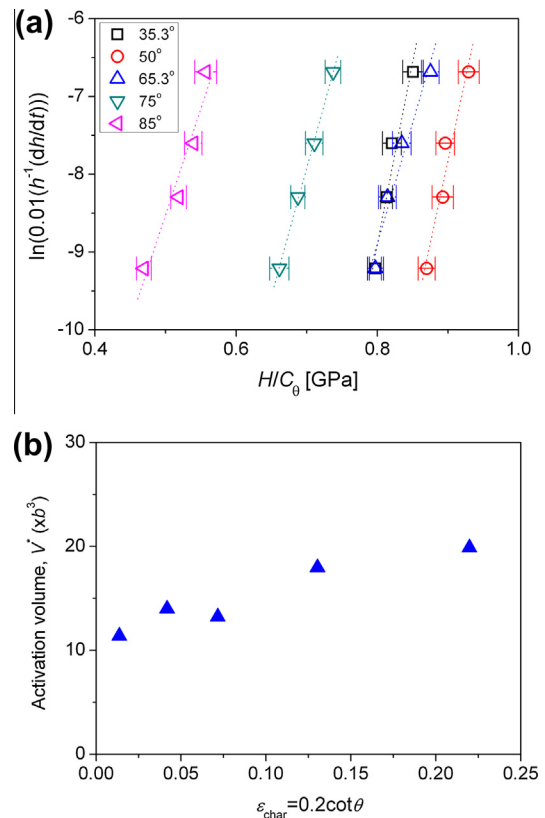


Fig. 11. Estimation of activation volume: (a) Logarithmic strain rate vs. linear stress for nt-Cu; (b) summary of estimated activation volume for nt-Cu.

Table 3  
Summary of contact angle, equivalent strain, SRS ( $m$ ) and activation volume ( $V^*$ ) measured in the present experiments.

Contact angle	35.3°	50°	65.3°	75°	85°
Equivalent strain	0.22	0.13	0.072	0.042	0.014
$m$	0.025	0.025	0.036	0.043	0.07
$V^*$	$\sim 20b^3$	$\sim 18b^3$	$\sim 13b^3$	$\sim 14b^3$	$\sim 12b^3$
Note	Detwinning is observed	N/A	Detwinning is observed	N/A	N/A

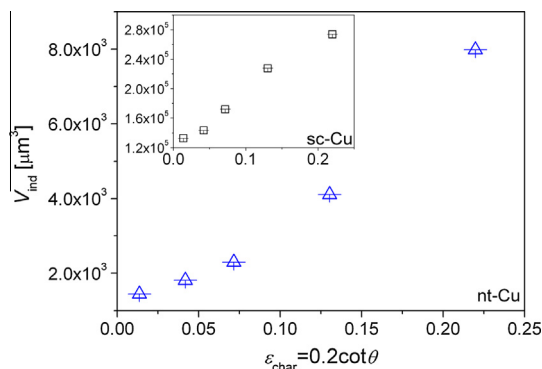


Fig. 12. Volume of the plastic zone of nt-Cu (and sc-Cu in the inset).

indenter [59], it is expected that all these deformation mechanisms are active during the nanoindentation experiments. At smaller strains (i.e., at the early stage of deformation), it is conceivable, however, that dislocation nucleation/emission or movement of pre-existing dislocations/kinks [45] could be predominant, leading to a higher  $m$  and a small  $V^*$  value ( $\sim 12b^3$ ), which are not commonly addressed in the literature. With the increasing strain, mechanisms such as slip-transfer and dislocation channeling processes are likely to play an increasing role, both of which mechanisms entail a relatively higher  $m$  and a modest  $V^*$  that are in accord with the present measurements. At even higher strain levels, the present authors notice from their experiments that localized detwinning occurs, giving rise to a very small  $m$  value that is not representative of nt structures. Owing to the lack of a unified picture on the detwinning and associated deformation kinetic parameters, further modeling is necessary to fully understand this behavior and the measured quantities.

From the nanoindentation technique point of view, an important question that is unresolved yet is: “How does the angle variation induce the trends of  $V^*$  and  $m$ ?” One possibility (although its detailed mechanism is not fully understood) may be associated with the volume of the plastic zone underneath the indenter. According to Johnson’s expanding cavity model for a conical indentation, the volume can be given as:

$$V_{\text{ind}} = \frac{2\pi r_p^3}{3} = \frac{2\pi a_c^3}{18(1-\nu)} \left[ \frac{E}{\sigma_y} \tan\left(\frac{\pi}{2} - \theta\right) + 4(1-2\nu) \right] \quad (8)$$

where  $r_p$  is the radius of plastic zone,  $a_c$  is the contact radius, and  $\nu$  is the Poisson’s ratio [60]. This equation suggests that, for a given indentation load, the volume of the transformed zone will increase with increasing sharpness

(or reducing angle), as shown in Fig. 12. Although there is no clue for correlating  $V_{\text{ind}}$  and  $V^*$ , similar trends are found in both volumes, i.e., each volume increases with decreasing  $\psi$ , and sc-Cu has much larger volume than nt-Cu. This may imply the possibility that, if it is assumed that indentation-induced plastic strain is accumulated by a similar number of thermally activated events, the probability of the occurrence of larger- $V^*$ -based events can be higher for larger  $V_{\text{ind}}$ . Again, however, this scenario is not fully understood at this point and needs further investigation.

## 5. Conclusions

Nanoindentation is a common technique for exploring the mechanical properties of nanostructured metals (nc, nt and ultrafine-grained materials), owing to the simplicity of the method and the relatively small amount of materials required. However, the influence of various indentation parameters on the measured mechanical properties is little known. Using nt-Cu as a model system, the present authors investigated the contact angle influence on the hardness, SRS and activation volume of nt-Cu (average  $\lambda \approx 40$  nm). Through a series of nanoindentation tests using five different indenters with different indenter angle and comparing the results with those of sc-Cu, it was found that the set of deformation parameters of nt-Cu depends sensitively upon the indenter types, in contrast to those of sc-Cu. At the smallest indenter angle (cube-corner indenter,  $\psi = 35.3^\circ$ ), which corresponds to the highest strains ( $\sim 0.22$ ), flow softening behavior, the lowest SRS ( $\sim 0.025$ ) and the largest activation volume ( $\sim 20b^3$ ) were observed. TEM investigations revealed detwinning and grain coarsening behavior under these nanoindentation conditions. However, high SRS ( $\sim 0.07$ ) and small activation volume ( $\sim 12b^3$ ) are observed for  $\psi = 85^\circ$ , in which conditions the deformation is likely to be dominated by the dislocation nucleation or motion of pre-existing partials/kinks. The variation in SRS by a factor of more than 3 using different indenters suggests that this variable is sensitive to the deformation conditions, and that caution is needed when comparing the various  $m$  values reported in the literature.

## Acknowledgements

This research was supported by Basic Science Research Program through the National Research Foundation of Korea (NRF) funded by the Ministry of Education, Science and Technology (No. 2010-0025526), and in part by

the Human Resources Development program (No. 20114010203020) of the Korea Institute of Energy Technology Evaluation and Planning (KETEP) grant funded by the Korea Government Ministry of Trade, Industry and Energy. The work at LLNL was performed under the auspices of the US Department of Energy by Lawrence Livermore National Security, LLC under Contract No. DE-AC52-07NA27344.

## References

- [1] Dao M, Lu L, Shen YF, Suresh S. *Acta Mater* 2006;54:5421.
- [2] Lu K, Lu L, Suresh S. *Science* 2009;324:349.
- [3] Kumar KS, Swygenhoven HV, Suresh S. *Acta Mater* 2003;51:5743.
- [4] Lu L, Chen X, Huang X, Lu K. *Science* 2009;323:607.
- [5] Zhang X, Misra A. *Scripta Mater* 2012;66:860.
- [6] Lu L, Shen Y, Chen X, Qian L, Lu K. *Science* 2004;304:422.
- [7] Lu L, Schwaiger R, Shan ZW, Dao M, Lu K, Suresh S. *Acta Mater* 2005;53:2169.
- [8] Wang YM, Hamza AV, Ma E. *Acta Mater* 2006;54:2715.
- [9] Asaro RJ, Suresh S. *Acta Mater* 2005;53:3369.
- [10] Shen YF, Lu L, Dao M, Suresh S. *Scripta Mater* 2006;55:319.
- [11] Ye JC, Wang YM, Barbee TW, Hamza AV. *Appl Phys Lett* 2012;100:261912.
- [12] Hodge AM, Wang YM, Barbee Jr TW. *Scripta Mater* 2008;59:163.
- [13] Carreker RP, Hibbard WR. *Acta Metall* 1953;1:656.
- [14] Follansbe PS, Kocks UF. *Acta Metall* 1988;36:81.
- [15] Shen YF, Lu L, Lu QH, Jin ZH, Lu K. *Scripta Mater* 2005;52:989.
- [16] Chen J, Lu L, Lu K. *Scripta Mater* 2006;54:1913.
- [17] Trelewicz JR, Schuh CA. *Acta Mater* 2007;55:5948.
- [18] Schwaiger R, Moser B, Dao M, Chollacoop N, Suresh S. *Acta Mater* 2003;51:5159.
- [19] Maier V, Durst K, Mueller J, Backes B, Höppel W, Göken M. *J Mater Res* 2011;26:1421.
- [20] Choi I-C, Yoo B-G, Kim Y-J, Seok M-Y, Wang YM, Jang J-i. *Scripta Mater* 2011;65:300.
- [21] Jang J-i, Lance MJ, Wen S, Tsui TY, Pharr GM. *Acta Mater* 2005;53:1759.
- [22] Jang J-i, Pharr GM. *Acta Mater* 2008;56:4458.
- [23] Shim S, Jang J-i, Pharr GM. *Acta Mater* 2008;56:3824.
- [24] Jang J-i, Yoo B-G, Kim Y-J, Oh J-H, Choi I-C, Bei H. *Scripta Mater* 2011;64:753.
- [25] Lucas BN, Oliver WC. *Metall Mater Trans A* 1999;30A:601.
- [26] Oliver WC, Pharr GM. *J Mater Res* 1992;7:1564.
- [27] Bezares J, Jiao S, Liu Y, Bufford D, Lu L, Zhang X, et al. *Acta Mater* 2012;60:4623.
- [28] Anderoglu O, Misra A, Ronning F, Wang H, Zhang X. *J Appl Phys* 2009;106:024313.
- [29] Vlassak JJ, Nix WD. *J Mech Phys Solids* 1994;42:1223.
- [30] Oliver WC, Pharr GM. *J Mater Res* 2004;19:3.
- [31] Strader JH, Shim S, Bei H, Oliver WC, Pharr GM. *Philos Mag* 2006;86:5285.
- [32] Bolshakov A, Pharr GM. *J Mater Res* 1998;13:1049.
- [33] Lee YH, Hahn JH, Nahm SH, Jang JI, Kwon D. *J Phys D: Appl Phys* 2008;41:074027.
- [34] Yoo BG, Park KW, Lee JC, Ramamurty U, Jang JI. *J Mater Res* 2009;24:1405.
- [35] Tabor D. *The hardness of metals*. Oxford: Oxford University Press; 1951.
- [36] Atkins AG, Tabor D. *J Mech Phys Solids* 1970;18:115.
- [37] Wang YM, Ott RT, van Buuren T, Willey TM, Biener MM, Hamza AV. *Phys Rev B* 2012;85:014101.
- [38] Johnson KL. *Contact mechanics*. Cambridge: Cambridge University Press; 1985.
- [39] Hertzberg RW. *Deformation and fracture mechanics of engineering materials*. New York: John Wiley; 1989.
- [40] Sakai M, Akatsu T, Numata S, Matsuda K. *J Mater Res* 2003;18:2087.
- [41] Mirshams RA, Pothapragada RM. *Acta Mater* 2006;54:1123.
- [42] Zhang K, Weertman JR, Eastman JA. *Appl Phys Lett* 2005;87:061921.
- [43] You Z, Li X, Gui L, Lu Q, Zhu T, Gao H, et al. *Acta Mater* 2013;61:217.
- [44] Maier V, Merle B, Göken M, Durst K. *J Mater Res* 2013;28:1177.
- [45] Wang YM, Sansoz F, LaGrange T, Ott RT, Marian J, Barbee Jr TW, et al. *Nat Mater* 2013;12:697.
- [46] Hodge AM, Furnish TA, Shute CJ, Liao Y, Huang X, Hong CS, et al. *Scripta Mater* 2012;66:872.
- [47] Shute CJ, Myers BD, Xie S, Li S-Y, Barbee Jr TW, Hodge AM, et al. *Acta Mater* 2011;59:4569.
- [48] Yu KY, Bufford D, Sun C, Liu Y, Wang H, Kirk MA, et al. *Nat Commun* 2013;4:1377.
- [49] Shabib I, Miller RE. *Acta Mater* 2009;57:4364.
- [50] Mayo MJ, Nix WD. *Acta Metall* 1988;36:2183.
- [51] Wang CL, Lai YH, Huang JC, Nieh TG. *Scripta Mater* 2010;62:175.
- [52] Choi I-C, Yoo B-G, Kim Y-J, Jang J-i. *J Mater Res* 2012;27:3.
- [53] Yoo B-G, Kim J-Y, Kim Y-J, Choi I-C, Shim S, Tsui TY, et al. *Int J Plast* 2012;37:108.
- [54] Choi I-C, Kim Y-J, Seok M-Y, Yoo B-G, Kim J-Y, Wang Y, et al. *Int J Plast* 2013;41:53.
- [55] Wang YM, Ma E. *Acta Mater* 2004;52:1699.
- [56] Zhu T, Li J, Samanta A, Kim HG, Suresh S. *Proc Natl Acad Sci USA* 2007;104:3031.
- [57] Conrad H. *Mater Sci Eng A* 2003;341:216.
- [58] Ma E. *Science* 2004;305:623.
- [59] Prasad KE, Chollacoop N, Ramamurty U. *Acta Mater* 2011;59:4343.
- [60] Johnson KL. *J Mech Phys Solids* 1970;18:115.